7-2015

Spatiotemporal fluctuations of olfactory stimuli and its detection by an optical method

Mitu Chandra Acharjee
University of Arkansas, Fayetteville

Spatiotemporal Fluctuations of Olfactory Stimuli and
its Detection by an Optical Method.

A thesis submitted in partial fulfillment
of the requirements for the degree of
Master of Science in Physics

by

Mitu Chandra Acharjee
Shahjalal University of Science and Technology
Master of Science in Physics, 2008

July 2015
University of Arkansas

This thesis is approved for recommendation to the Graduate Council.

Dr. Woodrow Shew
Thesis Director

Dr. Jiali Li
Committee Member

Dr. Pradeep Kumar
Committee Member

Dr. Julie A. Stenken
Committee Member

ABSTRACT

Olfactory processing in the mammalian brain is a highly dynamic process, yet most of the olfaction experiments have been studied primarily with static stimuli. Odors in the natural environment are transported by turbulent flow of air or water. Natural odorants have fluctuations in concentration and it changes rapidly with time. These rapid fluctuations may pose some challenges to identifying an odor; on the other hand, the variation itself may provide important clues about the odor source. The goal of this thesis project was to create a similar odorant environment like the rapid odor fluctuations encountered in nature – to meet this goal; we built an odor delivery and optical odor detection system. We combine visible smoke with invisible odorant to make the odorant detectable using two high sensitivity CCD line cameras. Initial tests of the system were carried out to determine the plausibility of its use in future experiments. Based on observed and quantified fluctuations of smoke and odorants, we conclude that the system is a promising tool for studying olfaction with naturalistic odorant fluctuations.

ACKNOWLEDGEMENTS

First of all, I would like to express my deep gratitude to my graduate advisor and thesis director, Dr. Woodrow Shew for providing me an opportunity to do this research project. In particularly, he laid the foundation for my work on olfactory system of mammals and every experimental result in this thesis bears a trace of his influence. His cheer and charisma, passion and compassion, together make him the most inspiring scientific communicator and leader I know. Without his support it would not have been possible for me to complete this project.

I am thankful to Dr. Jiali Li, Dr. Julie A. Stenken, Dr. Pradeep Kumar and Dr. Salvador Barraza-Lopez for being in my thesis committee. I am deeply indebted to all past and current group members for establishing the lab, shaping its culture for an excellent research environment.

I would like to thank Dick Penhallegon - Electronics Technician and Brandon Rogers – Machinist for providing the facilities to build the lab devices for measurements.

I owe one final acknowledgment to my wife and mother, whose love and support will never flag or fail.

TABLE OF CONTENTS

LIST OF FIGURES

1. INTRODUCTION

Many animals rely greatly on their olfactory system to categorize food sources, evaluate the social status within the species, and avoid predators. The odorants that give rise to these behaviors are complex mixtures of chemicals that must be represented as distinct patterns of activity by neurons in the olfactory system. The principles of encoding and discrimination of natural odor stimuli in the main olfactory bulb (MOB) , the first stage in the neural processing of volatile odorants[31] remain unclear.

Turbulent media such as air or water carries odors and creates fluctuations of concentrations of odorant. As a result, signals arriving at the olfactory sensors vary both in intensity and in duration[1]. Further fluctuations to the signal is added by sniffing, whisking, head movements and other active sampling behaviors[2,3].Odors of interest (e.g., food or mates) are usually classified within a fluctuating, multi-odor background[4–7] by the animal to locate their source. However, the extract encoding of identity and intensity of multiple odors extracted from the natural spatiotemporal fluctuations of odorants by the olfactory system is still unknown.

1.1 Thesis Overview

The motivation behind this thesis was to find neural response of olfactory bulb to the spatiotemporal fluctuations of olfactory stimuli and to relate the statistics of neural response to the statistics of stimulus. In chapter 1 the basic of olfactory system and the mechanism of olfactory coding is briefly described. Chapters 2 and 3 discuss the devices used to create and detect fluctuations of odorant molecules. Chapter 4 describes experimental results and finally, in chapter 5 the project is concluded and the possible future works are proposed.

1.2 Basic of Olfactory system

The sense of smell is commonly termed as Olfaction. General sensation of smell of a particular quality is known as Odor and any specific fragrant chemical is called odorant. Every chemical is not an odorant. Molecules must be volatile, small, and hydrophobic [25] to be sensed by the olfactory system. Nose is our only olfactory organ.

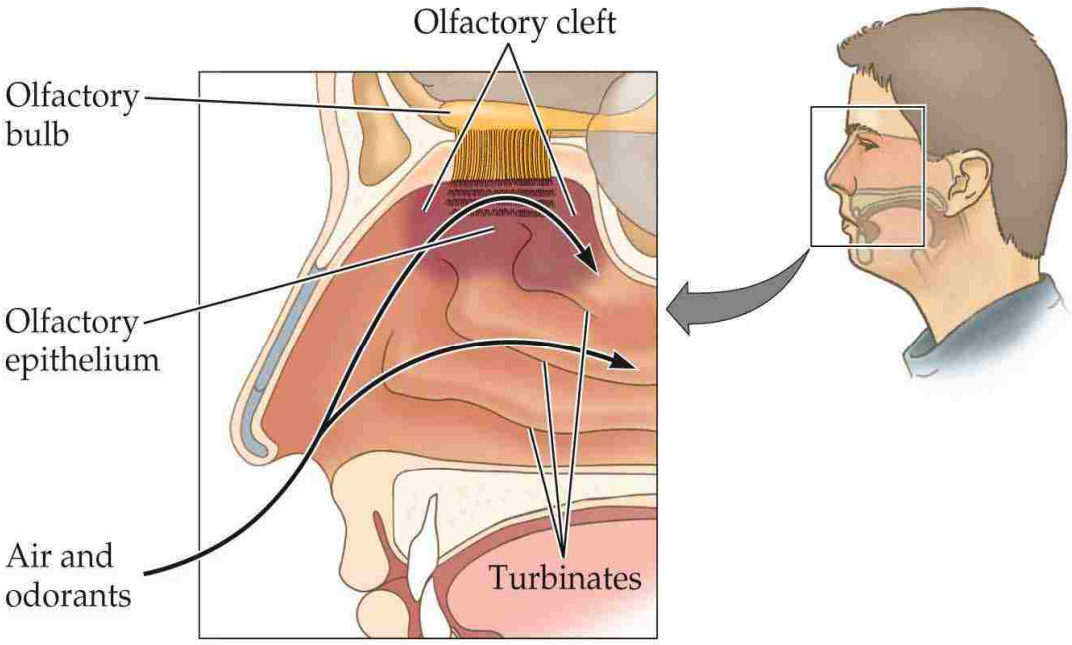

Figure 1.1. Human olfactory systems.[22]Inhaled air transports odorant chemicals into the epithelium. These signals are then transmitted to olfactory bulb and onward to other brain regions for further processing. Note that the concentration of odorants carried by the inhaled air is spatiotemporally fluctuating due to turbulent mixing in the outside environment.

Most of the mammals share a common internal olfactory system. Olfactory sensory system activates when odor molecules come in contact with particular processes known as the olfactory vesicles [26]. Olfactory epithelium consists of secretary mucosa which is known as the "retina of the nose". Detection of odorants is the primary function of olfactory epithelium which consists of three types of cell:

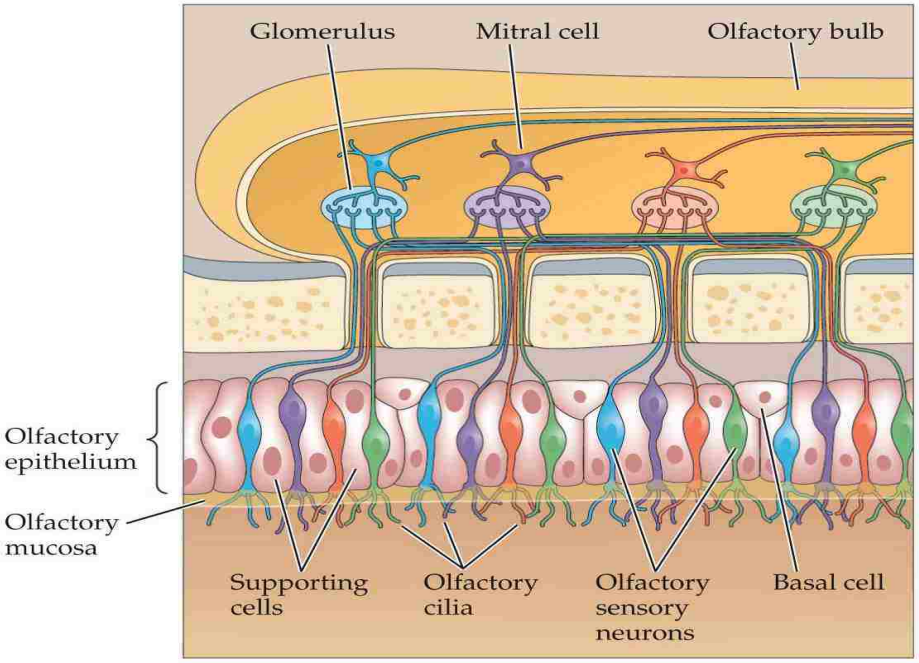

Figure 1.2. Cross-section of olfactory neural pathway between nose and olfactory bulb. [23]

The main cell type in the olfactory epithelium is the olfactory sensory neurons (OSNs). They are located below mucous layer in the epithelium. Unlike in retina, cochlea, skin, or tongue, they are the only kind of sensory receptors that make direct contact with physical stimulus. Hair like protrusions on OSN dendrites called cilia acts as a receptor of odorant molecules. They receive

and transfer olfactory signals to the upper parts of the brain .Odorant molecules bind on the olfactory receptor neurons on the OSNs. Initiation of an action potential requires binding of seven or eight odor molecules. Observation by a recent group suggests that the primary step in odor discrimination is mediated by ~ 1000 individual olfactory receptors [24].

1.3 How fast changes in odorant concentration are encoded

In the input layer (glomeruli) of the olfactory bulb (OB) odor identity is represented and well characterized. Individual olfactory receptor neurons (ORNs) have a selection for subsets of odors and projections of ORNs to glomeruli are conserved. As a result, spatiotemporal activity patterns on the OB surface[8–12] are formed which are different for individual odors. Inputs from multiple glomeruli are integrated by the local microcircuits which transforms the spatial distribution of glomerular patterns into temporal codes on Mitral/Tufted (M/T) cells[13]. The respiratory cycle responded by the phasic tuning of M/T cell which is known as respiration tuning[14, 15]. This response further increases the temporal variety of odor responses[16–18]. The variety of latencies of individual odors of M/T cell responses during respiration have been anticipated as a substrate for coding of individuality of odor which is known as latency coding.[19–21]

There are temporal variations in odor stimuli which challenge a temporal framework for coding of identical odors. M/T cell responses temporally modulate with the variations in concentrations of the odor stimuli. Additional glomeruli are recruited with the increase in concentrations in the stimuli[8–10, 12] which changes M/T cell firing patterns. M/T cells are likely to fire in advance in the respiratory cycle and show signs of comprehensive inhibitory responses[16, 32] with higher concentrations. Temporal shifts in M/T cell firing relating to

the respiratory cycle have been revealed to be distinctive of mixture responses[16, 33]. Odor mixtures activate glomerular activity patterns which usually go beyond the particular odor activation maps in the glomeruli[12, 34]. As a result, neither the behavioral percepts[35, 36] nor the particular M/T cell firing patterns[33] can be concluded as simple sums of the particular odors in a mixture. Therefore, M/T cell encoding is extremely controlled, since it must retain real-time data on spatiotemporal properties of individual odor, intensity, etc. Limitations in technical devices[37] in maintaining spatiotemporal fluctuations of odor stimuli have constrained the facility on olfactory experiments with natural odorants.

Most recently, one group have found that individual M/T cells respond in a surprisingly linear manner to temporally interleaved inputs of particular odors and their mixtures. Further, they showed that latency coding of spatiotemporal odor of M/T cells across the respiration cycle are growing properties of linear summation[38].

1.4 Turbulence creates odorant fluctuations

Wind disperses odor molecules from their source when odor plume formed. Their complex structure is much like that seen in smoke plumes. The plume spreads randomly over a wide area. Most of the animals and insects have the ability to track odor plumes to their source and this process helps them to find food and mate at distant sources . Odors are released from the source and odor plumes are formed when the molecules are spread by the wind. Since the odor plumes moves away from the source, it expands and the mean concentration of plumes falls. In a stable atmosphere at night under clear skies, buoyancy forces reduce turbulence and restrain its production.

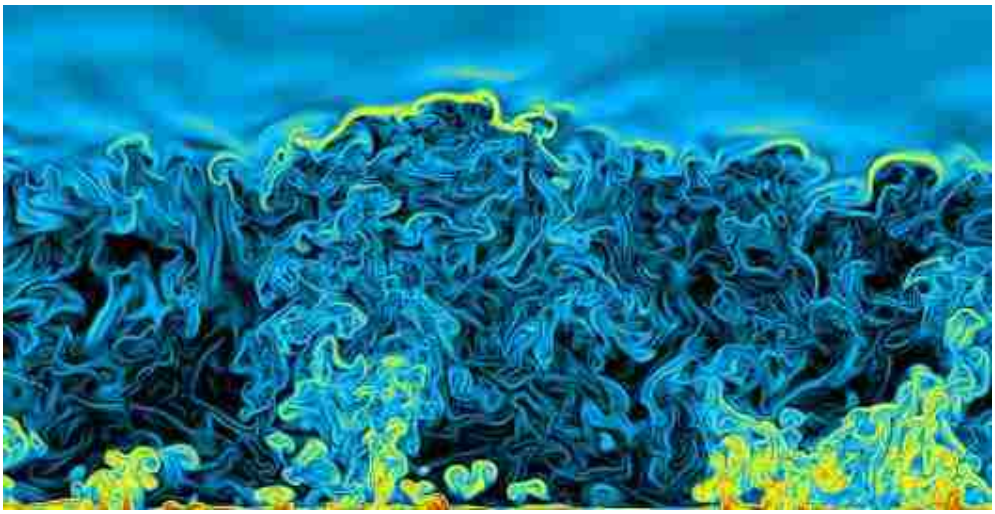

Figure 1.3. Visualization of air turbulences performed by Computer simulation at the Julich Supercomputing centre. Turbulences boundary layer is shown by vertical cross-section and the upper troposphere is the undulations due to the turbulences. Local variations of the density field is indicated by color variations, increasing from black to yellow to red.[44]

On the other hand in an unstable atmosphere, buoyancy forces promote the production of turbulence. Unstable conditions occur when heat from the sun rays is transmitted to the air at ground level and convective updrafts develop. Turbulence created by non-buoyancy forces is continued under neutral conditions. Transformation of energy continues from the massive vortices or eddies to smaller vortices. Vortices become more randomly oriented as they become smaller, until they show no favored direction. As a result the wind speed in a given direction fluctuates frequently. Viscous dissipation in the smallest eddies then removes the energy in the largest eddies injected by the turbulence. Viscosity of the air determines the size of the dissipation range of eddies and is characterized by the Kolmogoroff length which a measure of the size of the smallest turbulent motions. It is normally a centimeter or so in the atmosphere, and is approximately a function of wind speed and height[30].

Odor molecules released from a source smaller than the Kolmogoroff scale, will expand slowly by molecular diffusion until it reaches the size of the smallest eddies and the development of the plume depends on the characteristics of the odor molecules. The length plume growth of this molecular diffusion depends on source size and wind speed. In the case of a small source Miksad & Kittredge [30] found the length could be some meters which was argued by Aylor et al[27] .They showed that pheromone emitted by a female insect on the edge on a leaf, the source aerodynamically includes both leaf and insect and compares in size to the smallest eddies and this would probably not exceed a centimeter or so. Outside this point, the odor plume is independent of the material within it. Larger turbulence balances on a developing odor plume[28] when observed with tracers. The small-scale structure is determined by the eddies with size range from the Kolmogoroff length up to some hundreds of millimeters which stretch and stir the filaments in the plume[29].

The air inside our lab is turbulent due to the variations in the room temperature. So smoke-odor mixture when puffed went through this turbulent air. Air turbulence causes the fluctuations in the odor mixture which was detected by high sensitivity line camera.

2. DEVICE

2.1 Introduction

This chapter briefly discuss about the devices used in this thesis project for odor delivery and odor detection. Then precise control of the devices is discussed to obtain desired fluctuations in odorant. The last part of this chapter discussed about Schlieren imaging and optical detection of odorant fluctuations.

2.2 Odor delivery system

In order to make odorant molecule detectable by the optical sensor, we mixed them with smoke. The smoke is formed by a puffer which uses a liquid solution of ethylene glycol and glycerin to produce smoke. Ethylene glycol and glycerin are individually odorless and nonhazardous but when they burned together they generate smoky odor (Figure 2.2). The mixture of odor and smoke is kept in a Pyrex flask which is then puffed in between the scanner by a puffer system. Our puffer system included a computer-controlled pressure regulator (IP610-030, Omega Engineering Inc., CT, USA) connected to a compressed air source. Next to the pressure regulator was a small electro-mechanical valve (LHDA0531115H, The Lee Company, CT, USA). The pressure regulator, the valve, and data acquisition from the CCDs were organized with a Labview program and a NI 6343 acquisition system (National Instruments, TX, USA). We were able to tune puff pressure from zero to 30 PSI and the valve could be opened for any period which allows a wide range of puff strength. The examples shown in this paper were 1.0 sec in duration with a puff tube inner diameter of 1cm positioned 5.0 cm from the line camera (Figure 2.1).

2.3 Odor detection system

The mixture of smoke and odorant molecule puffed in between two line camera can be detected by optical sensors. The image formed in this case is a shadow of the mixture of smoke and odor. This image formation can be explained by the principle of Schlieren imaging.

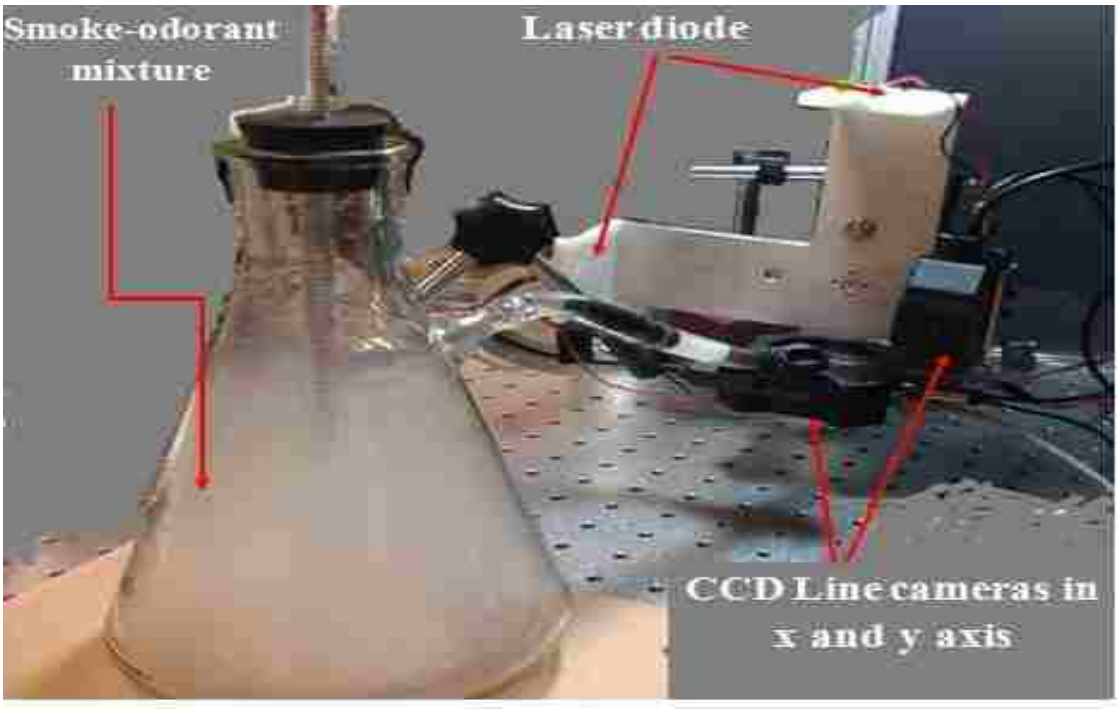

Figure 2.1. Odor fluctuation is detected based on shadows cast by the mixture of odor and smoke upon two CCD line cameras (up to 1000 images/sec, 1×2048 pixels, 14 μm/pixel resolutions). The light sources are laser diodes.

Figure 2.2. Smoke generator which uses a mixture of Ethylene glycol and glycerin to produce smoke [39].

Our odor detection is based on simple light scattering. The smoke passes between a laser diode light source and a linear CCD array (line camera), as illustrated schematically in Figure

2.3. The smoke particles are small (<1 micron) and, thus, scatter light in all directions. These results in less light reaching the CCD when the smoke is present compared to when the smoke is absent. The shadow of the smoke is what we are interested in detecting, because a darker shadow indicates a higher smoke concentration. Our technique is similar to, but different than Schlieren shadowgraphy as discussed in section 3.

2.3.1 Optical detection

We used optical sensors to capture the shadow cast by the mixture of odor and smoke, which is puffed between the sensors and a light source. The system is capable of capturing the motion of puffed smoke with millisecond temporal resolution, micron spatial resolution.

The odor detector involved two linear charge-coupled devices (CCD) each with 2048 pixels in a line and was able to capture one linear 'image' per 1.06 milliseconds (LC100, Smart Line Camera, Thorlabs Inc, NJ, USA). It was connected with a data gaining computer via USB and was supplied with Lab view drivers which allow easy incorporation into multifarious systems of experiments. Labview code helped us to control the CCDs in Supporting Information (SI). We were able to configure pressure regulator via Labview to provide a 0–5 V square pulse for each image acquired. The length of each pixel was 14 microns which provided a superb spatial resolution concluded the 2.87 cm length of each CCD. Figure 2.1 shows, a laser diode (650 nm, 5 mW, D650-5I, US Lasers Inc, CA, USA) located 17 cm from each CCD provides coherent point-source lighting of the whole CCD [40]. A rigid frame as shown in Figure 2.1 was used to mount two CCDs and two laser diodes.

3. SIMILAR DEVICES /METHODS

3.1 Introduction

This chapter briefly discusses about Schlieren imaging and photo ionization detectors (PID) to measure the concentration of volatile organic compounds directly in the sample. It also explains about working principles of PID and various applications in the field of science and technology. We will use PID to measure the concentrations in the fluctuations of the odorant.

3.2 Schlieren imaging

The physical basis for Schlieren imaging emerges from Snell's Law, which states that light, slows upon interaction with matter. If media is homogeneous, such as in a vacuum, or space, light travels uniformly, at a constant velocity. The density of an inhomogeneous media such as smokes in motion varies with time. And, the index of refraction changes with smoke density. When encountering such inhomogeneous media, variations in the refractive index deflect or phase shift light passing through the smoke, resulting in schliere. Slight deviations in a conventional Schlieren set-up can result in systems with distinct but informative optical representation of flow. One notable method is shadowgraphy.

Shadowgraphy is an optical technique which projects the shadow of an optical image onto a viewing plane for image capture [41]. The method of collecting shadowgraphs is similar to how humans visualize fluctuations in air density with their eyes, e.g. from the hood of an overheated car or gas rising from a barbecue grill [42]. A basic shadowgraph system consists of a light source and a light capturing device to project shadowgraph onto for observation, as shown in Figure 3.1. Because shadowgraphs are simply shadows of a Schlieren object, they can be magnified in accordance to their distance from the screen [41].

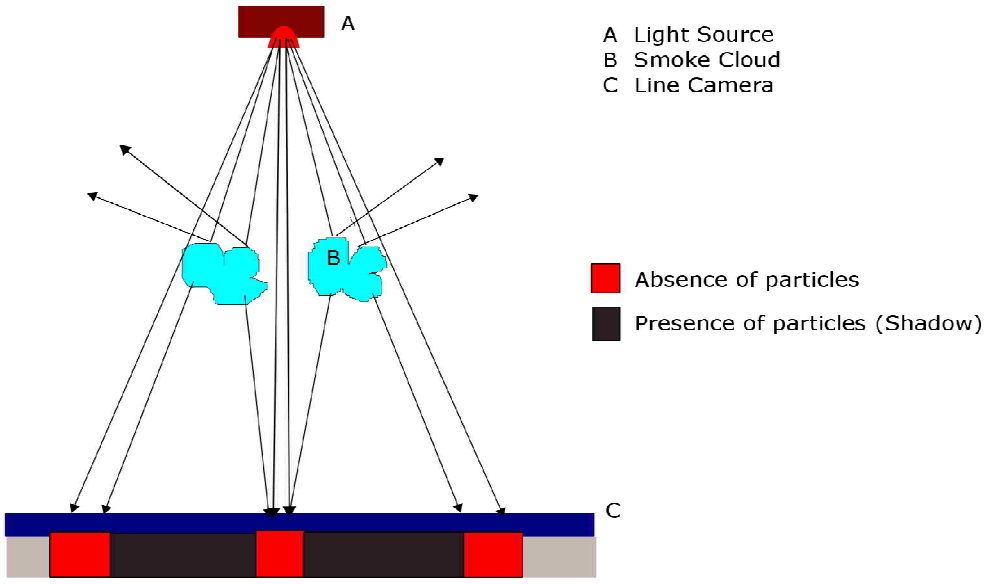

Figure 3.1. Formation of shadowgraph by the scattering of light ray from the smoke particles in motion.

In addition, the size and flexibility of a shadowgraph system construction is desirable in visualizing large-scale or extremely sensitive Schlieren objects [41].

3.2 Photo ionization Detector

The photo ionization detector (PID) is used to detect the concentrations of volatile organic compounds (VOCs). There is a lamp inside PID device which uses ultraviolet light to ionize gas molecules. The ionized molecules then used to measure the concentrations of the organic compounds [43].

There are portable PIDs (see Figure 3.2) which offer fast response and the ability to detect low gas concentrations. They are practical and reliable for the detection of VOCs.

Figure 3.2. A Pocket PID Monitor [43].

3.2.1 Principle of Operation

PID lamp is filled with a low-pressure inert gas which is energized with energy in resonance with the natural frequency of the gas molecules. As a result, an ultraviolet spectral radiation is produced. The emitted UV light shows a variety of wavelengths based on the type of gas in the lamp. Krypton is commonly used with other variety of gases. Figure 3.3 shows wavelengths emitted by argon, krypton, and. A t the discharge end of the lamp special crystal materials are used to allow spectral emissions to traverse. A pair of electrode biased with a stable DC voltage is placed in close proximity to the lamp window where the light is emitted. Ionization of gas molecules happens when they enter on the radiated field in the space between the electrodes and the free electrons are stored at the electrodes. As a result, a current flows whose magnitude is directly proportional to the gas concentration [43].

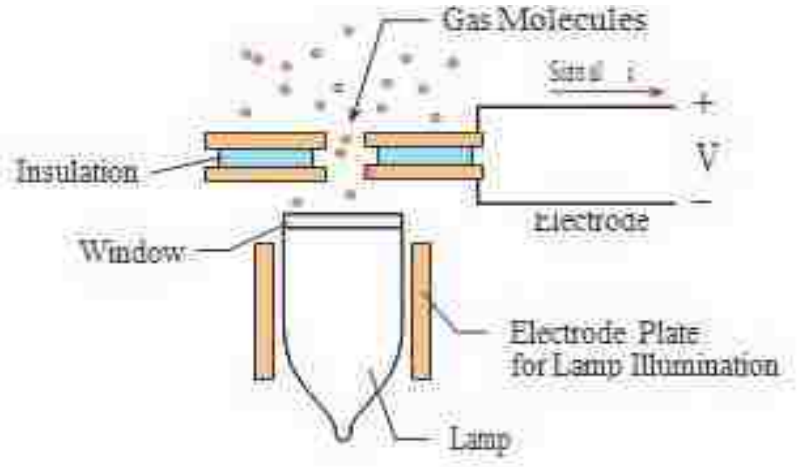

Figure 3.3. Typical Photo ionization Detector Configuration [43].

3.2.2 Applications

PID devices are recommended for fast response, high accuracy, and good sensitivity for detection of volatile organic compounds (VOCs). They are not recommended for use in stationary monitors, which sample continuously since PID sensors involve intermittent cleaning and have limited life expectancies. Portable models are useful only where periodic readings are required [43].

4. RESULTS AND DISCUSSIONS

4.1 Introduction

This chapter briefly describes the results we found from our odor delivery and detecting system. We used the system to visualize a brief (1 s) puff of smoke and odorant. The visualization of odorant fluctuations is presented as image and plots using Matlab program.

4.2 Optical image of odorant fluctuations

Each line camera is capable of collecting linear 'images' at up to 1000 frames per second. The frame rate is set by the user via the Labview interface. For the purposes of our study we acquired one image every 1.9 ms from both line cameras. We collected 1000 images and stored the data in a 2048×1000 matrix (2048 pixels x 1000 images). This provided a total recording duration of 1.9 s, during which the puff of smoke and odorant was delivered. Labview was used to write the data to disk. We used Matlab to analyze the data. The first step in this analysis was to subtract the background baseline from every image (Figures 4.1 & 4.2). This was necessary because the laser diodes did not produce spatially uniform light. The baseline was defined and calculated as the mean of first 50 scans (when no smoke was present). Deviations from baseline are due to light scattering by the smoke. The subtracted data sets are used to create images in Matlab to visualize the fluctuations of concentration in the mixture of smoke and odorant. The image (Figure 4.5) is a representation of 2048×1000 matrix with pixels on the y axis and time on the x axis. Color indicates baseline-subtracted light intensity measured by the line cameras. Variations of light intensity are due to scattering from smoke particles .The puffing started at ~0.6 sec and continues until ~1.7 sec. Before puff started the baseline-subtracted light intensity was ~0 (yellow), Figure 4.5.

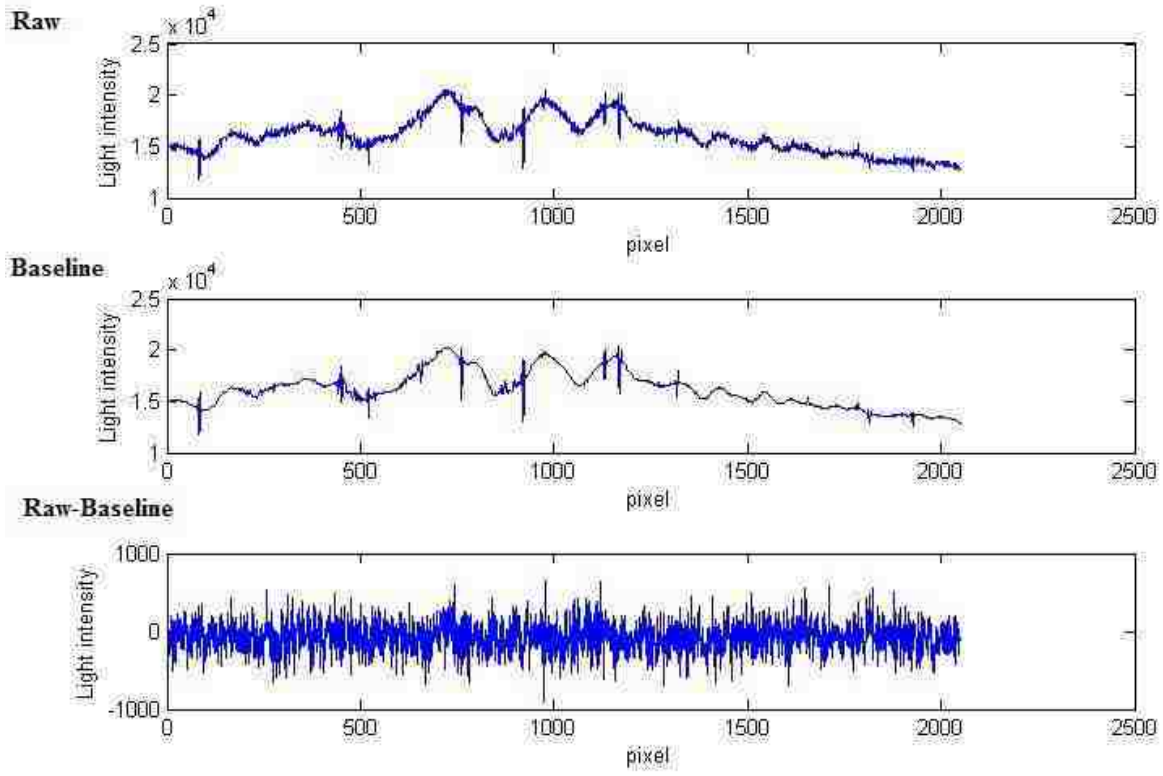

Figure 4.1. Each line in this figure represents one image from one of the line cameras when no smoke was present. The vertical axis is light intensity (in arbitrary units, a.u.); the horizontal axis is spatial distance (in pixels). (TOP) The light intensity fluctuations in this image are due to spatial inhomogeneity of the light source. No smoke is present. (MIDDLE) The baseline image is defined as the average of 50 single images like the one shown in the top panel. (BOTTOM) After subtracting the baseline, the remaining fluctuations are small and define the noise floor of our measurement system. The noise is most likely electrical in nature and varies randomly from one image to another.

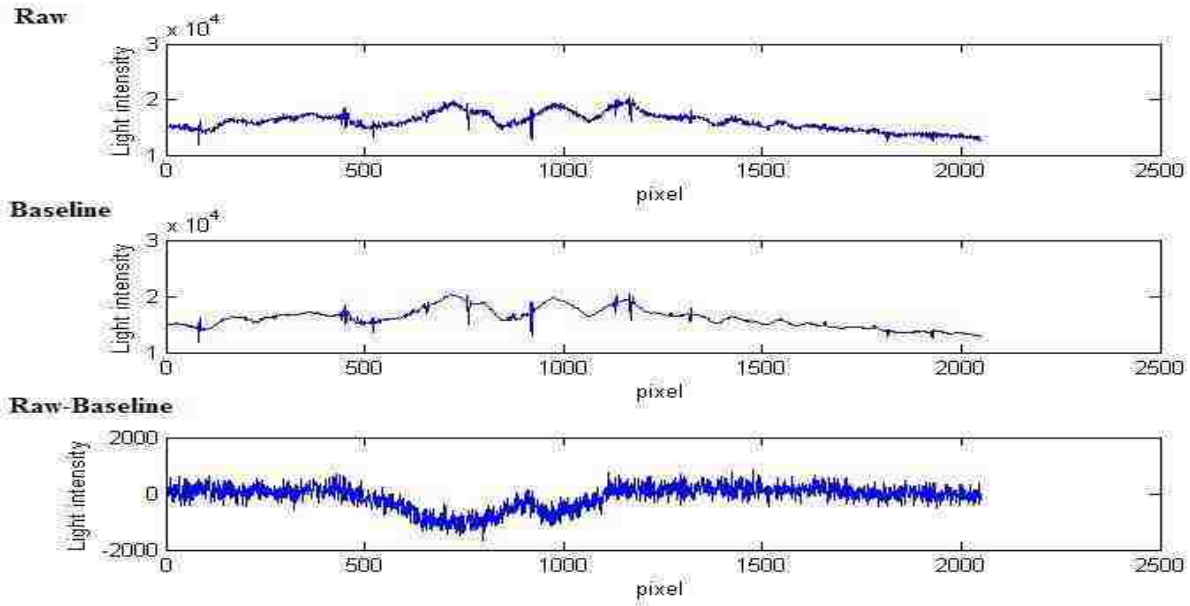

Figure 4.2. Subtraction of raw data from the baseline in the presence of smoke and odorant mixture. Fluctuations of odorant concentrations are clearly visible in the subtracted line.

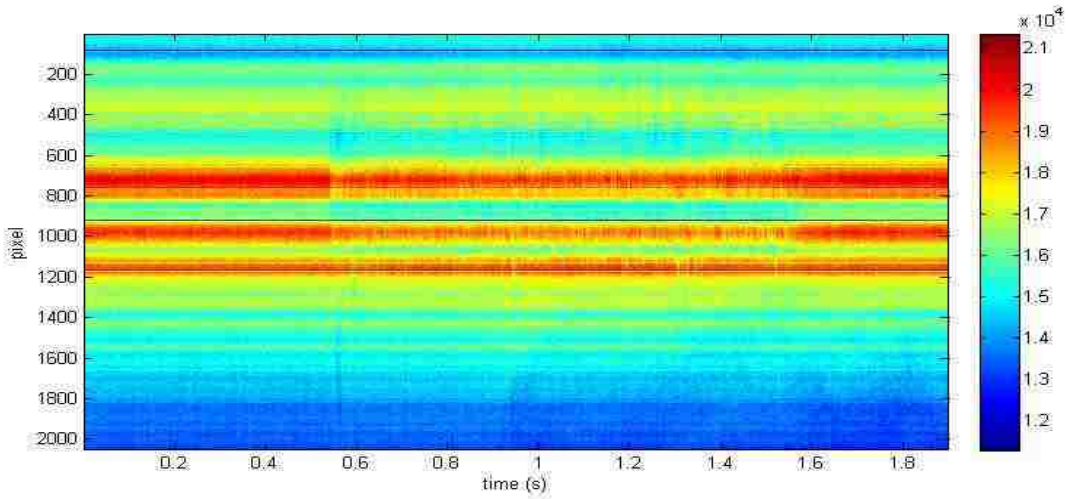

Figure 4.3. This figure displays 1000 images acquired from one line camera during 1.9 s. Each image comprises one column of this figure. Color indicates light intensity recorded by the camera. Thus, one row of this figure shows how light intensity of one camera pixel changes in time (with 1.9 ms temporal resolution). This data has not yet been subtracted by the baseline. The spatial irregularities of the raw scan are due primarily to non-uniform illumination from the laser diode light sources.

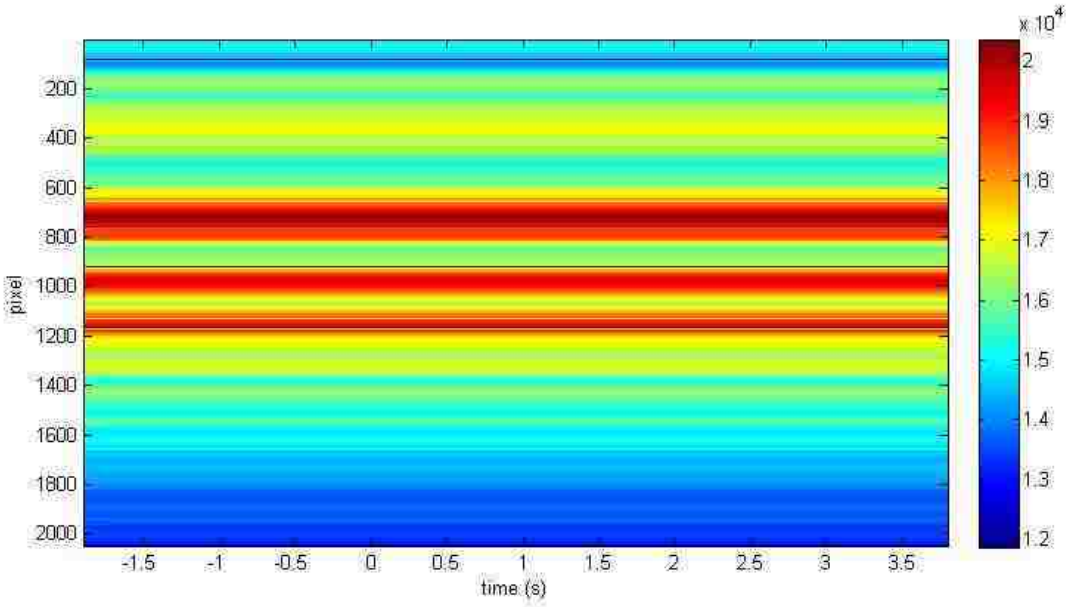

Figure 4.4. 1000 baseline images. This matrix is subtracted from that in Fig 4.3 in order to obtain Fig 4.5.

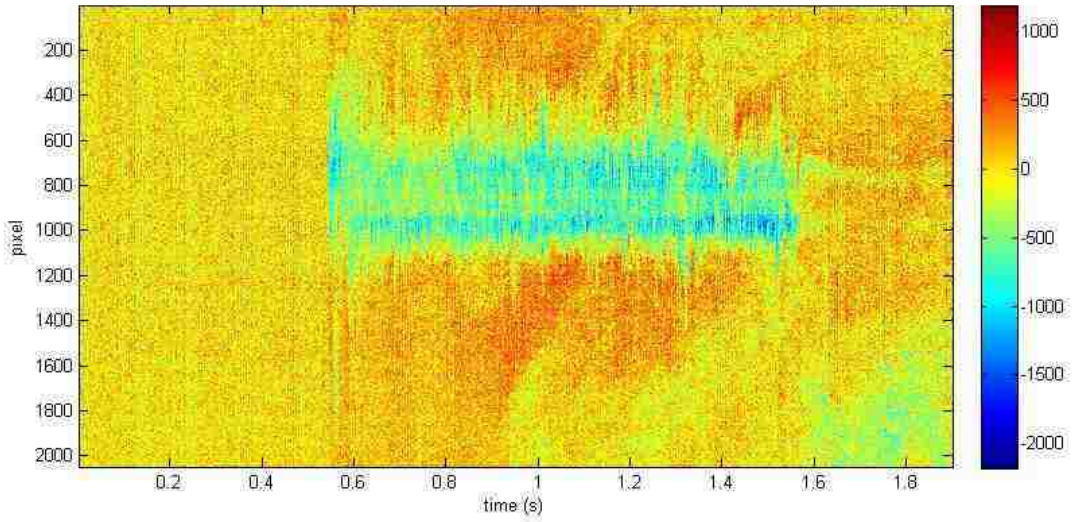

Figure 4.5. Static spatial irregularities of the light source are removed by subtracting the baseline (Fig 4.4) from the original data (Fig 4.3). The remaining fluctuations now clearly reveal the spatiotemporal dynamics of the smoke as it passes the line camera.

The region from 0.6 sec to 1.6 sec is covered with blue, red and yellow colors. Yellow is the color of the baseline which represents the state of the scanner before puffing smoke. On the

image, it is shown before 0.6 sec. Because of the background noise (electrical, mechanical or any other types), there were some initial fluctuations. As a result, the image before puff started was covered with yellow and some tiny red spots. When we subtracted pixels from the baseline some of the pixels went below baseline which indicated lower light intensity (marked by blue) and some other went above baseline which indicated higher light intensity (marked by red).Now, when the puff started (after 0.6 sec), it flowed over the scanner and made spatiotemporal fluctuations. Blue color on the image, represented the presence of smoke particles which was the shadow of the particles on the scanner. The surrounding red colors were due to the scattering of light from the smoke particles which intensified the light coming from the source and falling directly on the scanner. The spatiotemporal fluctuations of the smoke-odorant mixture were clearly visible on the image as the puff continued to ~1.9 sec.

4.2.1. Quantifying concentration statistics

Smoke-odor mixture was puffed through 5mm plastic tube at a distance of 5cm from the optical sensors. When we puffed in the central region bounded by the two optical sensors, we observed good fluctuations, roughly comparable to the fluctuations expected for natural odors.

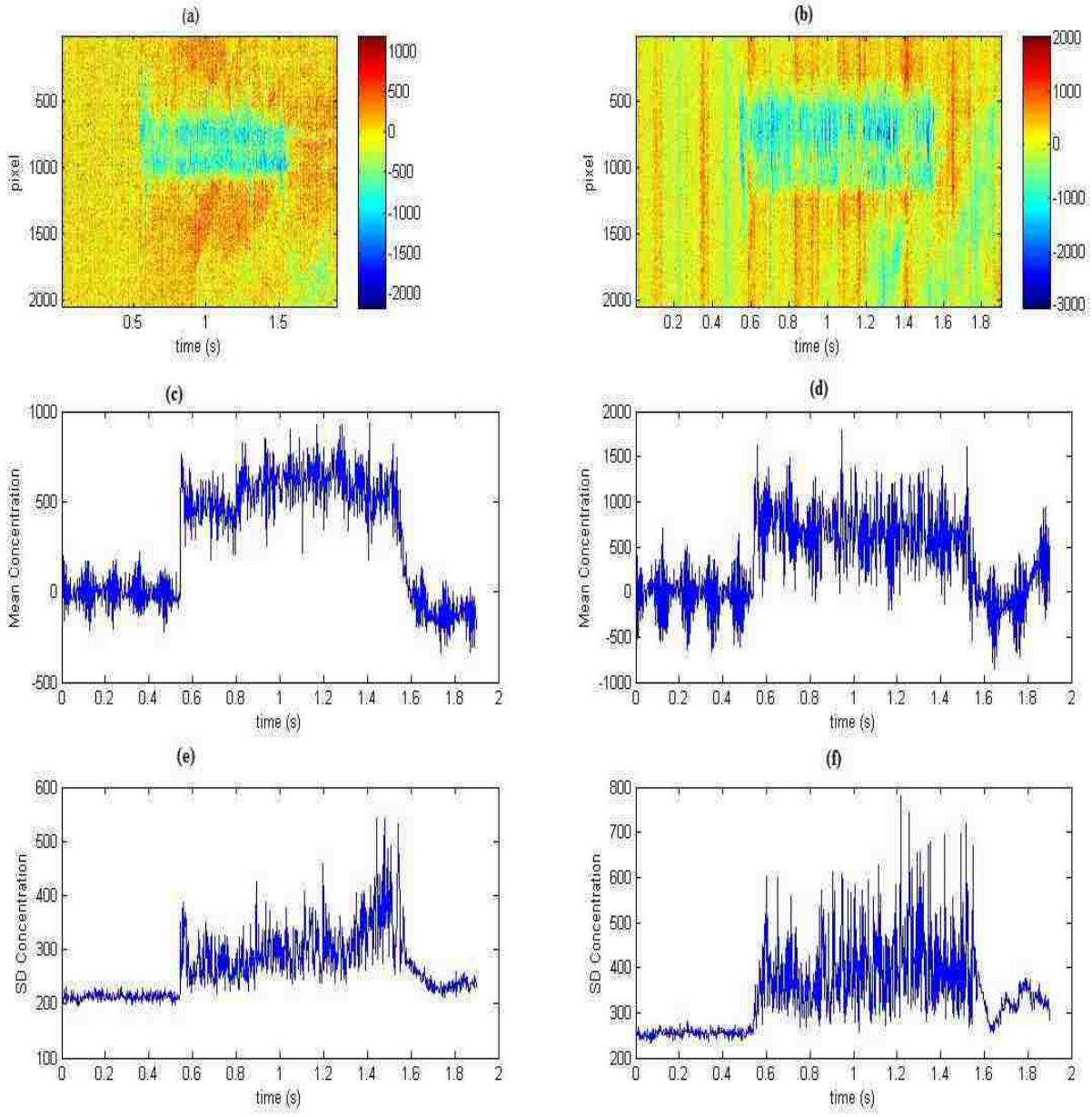

Figure 4.6. The data shown in this figure come from two line cameras oriented at a right angle to each other. The 'x camera' data is shown in panels a, c, e. The 'y camera' data is shown in panels b, d, f. (a) Image of puff captured by line camera on 'x' axis (b) Image of same puff simultaneously captured by line camera on' y' axis (c) Time series of fluctuations of mean x concentration within the region through which the smoke passed (pixels 600-1100) (d) Fluctuations of mean y concentration (mean over pixels 500-1200) (e) & (f) Note that the concentration across the averaged pixels is not uniform standard deviation(SD) of concentration along 'x' axis & 'y' axis.

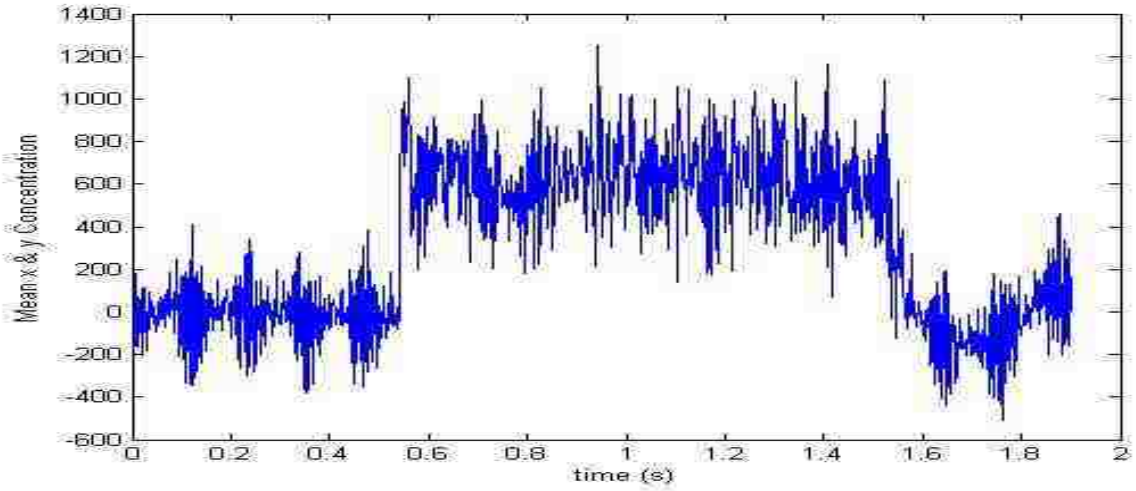

Figure 4.7. The data from the x and y cameras provides related, but not identical information about the smoke concentration within the measurement volume. To better approximate this concentration, we averaged the concentrations of x and y axis (Fig 4.6c and 4.6d). Shown is the time series of this x-y average.

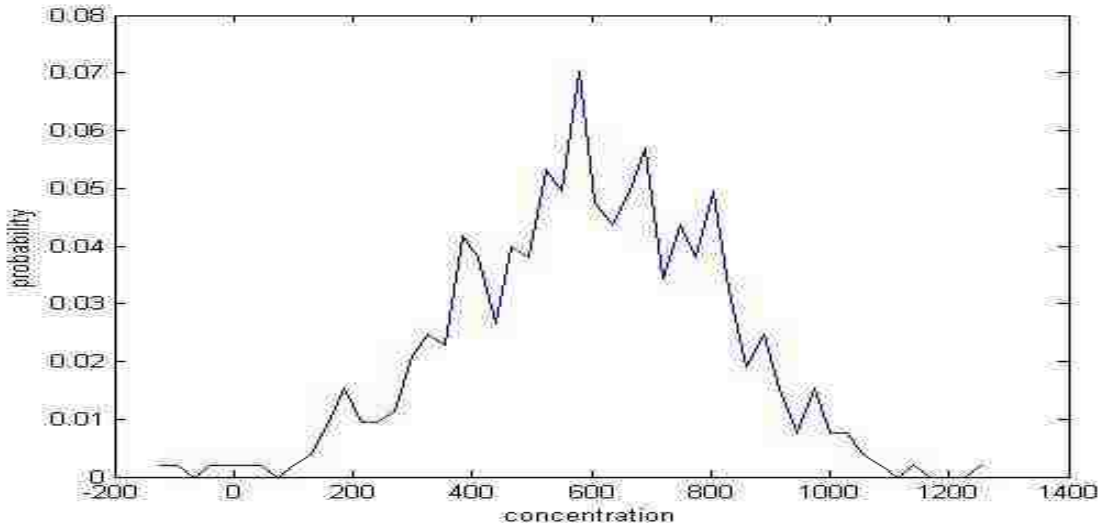

Figure 4.8. Our study is motivated by the fact that odors fluctuate in the natural world. Here we make an initial step towards quantifying the statistics of the fluctuations generated by our system. Shown is a probability distribution of mean x-y concentration within the measurement volume (based on the time series shown in Figure 4.7). This result demonstrates that the fluctuations (width of distribution) are comparable to the mean (center of the distribution). Therefore, conventional studies of the olfactory system should better account for odorant fluctuations. In future studies our system may be a useful tool for this goal.

5. CONCLUSION AND FUTURE WORK

5.1 Conclusion

The olfactory system must perform multiple tasks including odor identification and concentration detection. If there multiple odor present odor segmentation must also be performed. It many animals (not so much in humans), localization of odor sources, like food and mates, is also essential. Fluctuations in the odors concentration may play an important role in all of these activities. Based on the high and low concentrations, animals can decide how far or close the food source is. To better study the role of odor fluctuations in olfaction we need a reliable odor delivery system which can imitate natural spatiotemporal odor fluctuations. Only Then we can have study how the olfactory system of animal works with natural spatiotemporal fluctuation of odors. The system we have developed here may serve this purpose.

5.2 Future Work

In this thesis, we developed and explained a basic experimental system to produce spatiotemporal odorant fluctuations and optical detection of the fluctuation. This set up is very cost effective. However, some limitations of our device include the inability to precisely measure concentration in units such as mol/l. Rather; we can only see relative changes compared to baseline in arbitrary units. This limitation could be mitigated in future experiments using a PID device to calibrate our optical measurements. In addition the spatial resolution is not capable of measure concentration accurately in volumes smaller than about 5 mm x 5 mm x 5 mm. Finally, a significant limitation of our approach is that the odorant must be mixed with a visible medium like smoke. Nonetheless, future experiments could be performed with our device to deliver spatiotemporal odorant fluctuations to the rodent nostrils.

Together with recordings of electrophysiological neural activity of olfactory bulb and olfactory cortex, our device opens interesting possibilities for future work. Our device could reveal a statistical relation between the spatiotemporal fluctuations of odors and the neural activity .This may provide us an improved understanding of, how the olfactory system encodes natural odorants with spatiotemporal fluctuations.

REFERENCES

1. Crimaldi, J.P., Wiley, M.B. & Koseff, J.R. The relationship between mean and instantaneous structure in turbulent passive scalar plumes. *J. Turbul.* **3**, 014 (2002).

2. Vickers, N.J. Mechanisms of animal navigation in odor plumes. *Biol. Bull.* **198**, 203–212 (2000).

3. Koehl, M.A.R. The fluid mechanics of arthropod sniffing in turbulent odor plumes. *Chem. Senses* **31**, 93–105 (2006).

4. Wallace, D.G., Gorny, B. & Whishaw, I.Q. Rats can track odors, other rats, and themselves: implications for the study of spatial behavior. *Behav. Brain Res.* **131**, 185–192 (2002).

5. Uchida, N. & Mainen, Z.F. Speed and accuracy of olfactory discrimination in the rat. *Nat. Neurosci.* **6**, 1224–1229 (2003).

6. Rajan, R., Clement, J.P. & Bhalla, U.S. Rats smell in stereo. *Science* **311**, 666–670 (2006).

7. Khan, A.G., Sarangi, M. & Bhalla, U.S. Rats track odour trails accurately using a multi-layered strategy with near-optimal sampling. *Nat. Commun.* **3**, 703 (2012).

8. Rubin, B.D. & Katz, L.C. Optical imaging of odorant representations in the mammalian olfactory bulb. *Neuron* **23**, 499–511 (1999).

9. Meister, M. & Bonhoeffer, T. Tuning and topography in an odor map on the rat olfactory bulb. *J. Neurosci.* **21**, 1351–1360 (2001).

10. Spors, H. & Grinvald, A. Spatio-temporal dynamics of odor representations in the mammalian olfactory bulb. *Neuron* **34**, 301–315 (2002).

11. Soucy, E.R., Albeanu, D.F., Fantana, A.L., Murthy, V.N. & Meister, M. Precision and diversity in an odor map on the olfactory bulb. *Nat. Neurosci.* **12**, 210–220 (2009).

12. Fletcher, M.L. *et al.* Optical imaging of postsynaptic odor representation in the glomerular layer of the mouse olfactory bulb. *J. Neurophysiol.* **102**, 817–830 (2009).

13. Wilson, R.I. & Mainen, Z.F. Early events in olfactory processing. *Annu. Rev. Neurosci.* **29**, 163–201 (2006).

14. Adrian, E.D. Olfactory reactions in the brain of the hedgehog. *J. Physiol. (Lond.)* **100**, 459–473 (1942).

15. Macrides, F. & Chorover, S.L. Olfactory bulb units: activity correlated with inhalation cycles and odor quality. *Science* **175**, 84–87 (1972).

16. Khan, A.G., Thattai, M. & Bhalla, U.S. Odor representations in the rat olfactory bulb change smoothly with morphing stimuli. *Neuron* **57**, 571–585 (2008).

17. Dhawale, A.K., Hagiwara, A., Bhalla, U.S., Murthy, V.N. & Albeanu, D.F. Non-redundant odor coding by sister mitral cells revealed by light addressable glomeruli in the mouse. *Nat. Neurosci.* **13**, 1404–1412 (2010).

18. Fukunaga, I., Berning, M., Kollo, M., Schmaltz, A. & Schaefer, A.T. Two distinct channels of olfactory bulb output. *Neuron* **75**, 320–329 (2012).

19. Junek, S., Kludt, E., Wolf, F. & Schild, D. Olfactory coding with patterns of response latencies. *Neuron* **67**, 872–884 (2010).

20. Schaefer, A.T. & Margrie, T.W. Spatiotemporal representations in the olfactory system. *Trends Neurosci.* **30**, 92–100 (2007).

21. Laurent, G. *et al.* Odor encoding as an active, dynamical process: experiments, computation, and theory. *Annu. Rev. Neurosci.* **24**, 263–297 (2001).

22. Chapter 8: psych 310. *Study Blue* (2012). at <http:// www.studyblue.com/notes/note/n/psych-310-chapter-14/deck/3062119 >

23. Astroglia, *A Sense of smell* (2011). at <https://astroglia.wordpress.com/2012/09/06/a-sense-of-smell>

24. Kajiya, K., Inaki, K., Tanaka, M., Haga T., Kataoka, H.,& Touhara, K., Molecular Bases of Odor Discrimination: Reconstitution of Olfactory Receptors that Recognize Overlapping Sets of Odorants. *J. Neurosci* **21**, 6018-6025 (2001)

25. Pillow, J., Perception (PSY 323) Fall 2009.(2009)

26. Díaz D., Gómez C., Muñoz-Castañeda R., Baltanás F., Alonso JR., Weruaga E. The olfactory system as a puzzle: playing with its pieces. *Anat Rec (Hoboken)*. **296**, 1383-400 (2013).

27. Aylor, D.E., Parlange, J.Y., Grannett, J. Turbulent dispersion of dis- parlure in the forest and male gypsy moth response. *Environ . Entomol.* **5**, 1026-32 (1976)

28. Hanna, S.R., Insley, E.M. Time series analyses of concentration and wind fluctuations. *Boundary-Layer Meteorol*. **47**, 131-47 (1989)

29. Jones, C.D. On the structure of instantaneous plumes in the atmosphere. *J. Hazard. Mater*. **7**, 87-112 (1983)

30. Miksad, R.W., Kittredge, J. Pheromone aerial dispersion: a filament model. *In 14th Conf Agriculture and Forest Meteorology*. 23S·A3 (1979)

31. Yu, D.L., Shea, S.D., Katz, L.C. Representation of Natural Stimuli in the Rodent Main Olfactory Bulb. *Neuron*. **50**, 937–949 (2006)

32. Chalansonnet, M. & Chaput, M.A. Olfactory bulb output cell temporal response patterns to increasing odor concentrations in freely breathing rats. *Chem. Senses* **23**, 1–9 (1998).

33. Giraudet, P., Berthommier, F. & Chaput, M. Mitral cell temporal response patterns evoked by odor mixtures in the rat olfactory bulb. *J. Neurophysiol.* **88**, 829–838 (2002).

34. Lin, D.Y., Shea, S.D. & Katz, L.C. Representation of natural stimuli in the rodent main olfactory bulb. *Neuron.* **50**, 937–949 (2006).

35. McNamara, A.M., Magidson, P.D. & Linster, C. Binary mixture perception is affected by concentration of odor components. *Behav. Neurosci.* **121**, 1132–1136 (2007).

36. Frederick, D.E., Barlas, L., Ievins, A. & Kay, L.M. A critical test of the overlap hypothesis for odor mixture perception. *Behav. Neurosci.* **123**, 430–437 (2009).

37. Vetter, R.S., Sage, A.E., Justus, K.A., Cardé, R.T. & Galizia, C.G. Temporal integrity of an airborne odor stimulus is greatly affected by physical aspects of the odor delivery system. *Chem. Senses*. **31**, 359–369 (2006).

38. Gupta, P., Albeanu, D.F. & Bhalla, U.S. Olfactory bulb coding of odors, mixtures and sniffs is a linear sum of odor time profiles. *Nature Neuroscience.* **18**, 272–281(2015)

39. Zerotoys, *Dragon Puffer Air Flow Indicator*.(2015)at <http://www.zerotoys.com/product-p/dragonpuffer.htm>

40. Grady, S.K., Hoang, T.T., Gautam, S.H., Shew, W.L. Millisecond, Micron Precision Multi-Whisker Detector. *PLoS One*. 8, e73357 (2013)

41. Settles, G.S. Schlieren and Shadowgraph Techniques: Visualizing Phenomena in Transparent Media. *Springer*, 2 ed., 2006.

42. Wetzstein, G., Raskar, R., and Heidrich,W. Hand-held schlieren photography with light field probes.*IEEE International Conference on Computational Photography ICCP*, 2011.

43. Intlsensor , (2008). at <http://www.intlsensor.com/pdf/photoionization.pdf >

44. Juan, M.P., (2015). at < http://www.gauss-centre.eu/gauss-centre/EN/Projects/EnvironmentEnergy/2014/mellado_turb_mixing.html?nn=1236240 >

Appendix

Matlab Programs

```
B=importdata('xaxis3');
A=mean(B(:,1:50),2);
for i=1:1000
   C(:,i)=B(:,i)-A(:,1);
end
figure(2)
imagesc((1:1000)*0.0019,1:2048, C);

colorbar;
colormap(jet(128))
xlabel('time (s)')
ylabel('pixel')

figure(3)
subplot(311)
plot(B(:,600))
xlabel('pixel')
ylabel('Light intensity')

subplot(312)
```

```
plot(A)
xlabel('pixel')
ylabel('Light intensity')
subplot(313)
plot(C(:,600))
xlabel('pixel')
ylabel('Light intensity')
```